Journal of Coordination Chemistry

ISSN: 0095-8972 (Print) 1029-0389 (Online) Journal homepage: http://www.tandfonline.com/loi/gcoo20

Equilibria in the acidified aqueous dimethylformamide solutions of tungstate anion. Synthesis, crystal structure and characterization of novel decatungstate $[Ba(H_2O)_2(C_3H_7NO)_3]_2[W_{10}O_{32}]\cdot(C_3H_7NO)_2$

Olena Yu. Poimanova, Sergii V. Radio, Katerina Ye. Bilousova, Vyacheslav N. Baumer & Georgiy M. Rozantsev

To cite this article: Olena Yu. Poimanova, Sergii V. Radio, Katerina Ye. Bilousova, Vyacheslav N. Baumer & Georgiy M. Rozantsev (2015) Equilibria in the acidified aqueous dimethylformamide solutions of tungstate anion. Synthesis, crystal structure and characterization of novel decatungstate $[Ba(H_2O)_2(C_3H_7NO)_3]_2[W_{10}O_{32}]\#(C_3H_7NO)_2$, Journal of Coordination Chemistry, 68:1, 1-17, DOI: 10.1080/00958972.2014.987136

To link to this article: http://dx.doi.org/10.1080/00958972.2014.987136

Accepted author version posted online: 14 Nov 2014.
Published online: 08 Dec 2014.

Journal of Coordination Chemistry, 2015
Vol. 68, No. 1, 1–17, http://dx.doi.org/10.1080/00958972.2014.987136

Equilibria in the acidified aqueous dimethylformamide solutions of tungstate anion. Synthesis, crystal structure and characterization of novel decatungstate $[Ba(H_2O)_2(C_3H_7NO)_3]_2[W_{10}O_{32}]\cdot(C_3H_7NO)_2$

OLENA YU. POIMANOVA†, SERGII V. RADIO†, KATERINA YE. BILOUSOVA†, VYACHESLAV N. BAUMER‡§ and GEORGIY M. ROZANTSEV*†

†Faculty of Chemistry, Department of Inorganic Chemistry, Donetsk National University, Donetsk, Ukraine
‡State Scientific Institution "Institute for Single Crystals" of NAS of Ukraine, Kharkov, Ukraine
§Faculty of Chemistry, Department of Inorganic Chemistry, V.N. Karazin National University, Kharkiv, Ukraine

(*Received 26 August 2014; accepted 30 October 2014*)

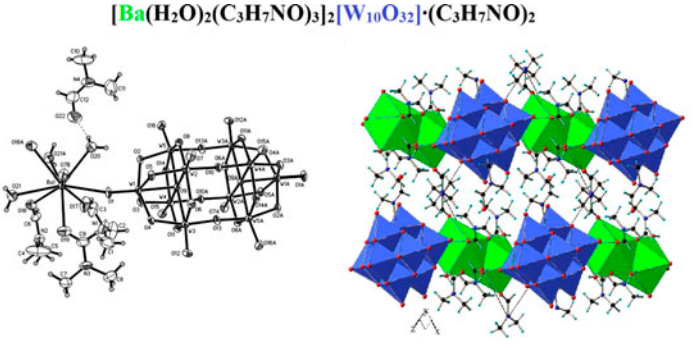

The formation and transformation of isopolytungstates in the system Na_2WO_4–HCl–NaCl–DMF–H_2O with different dimethylformamide (DMF) concentrations have been studied by single-point pH-potentiometric titration and the subsequent modeling of the equilibria processes. The modeling of equilibria resulted in data necessary to synthesize barium decatungstate, $[Ba(H_2O)_2(C_3H_7NO)_3]_2[W_{10}O_{32}]\cdot(C_3H_7NO)_2$. The salt was characterized by elemental and EDX spectral analysis, SEM, FT-IR spectroscopy, thermal analysis, single-crystal X-ray diffraction analysis in solid state, and by UV–vis spectroscopy in solution.

Keywords: Ionic equilibria; Isopolytungstate; Aqueous dimethylformamide solution; Barium(II) decatungstate; Crystal structure

1. Introduction

Due to the application of isopolytungstates (IPT) in different fields of science and technology [1], the problem of creating reproducible and targeted techniques for IPT

*Corresponding author. Email: g.rozantsev@donnu.edu.ua

synthesis arises. This requires a preliminary study of the state of isopolytungstate anions (IPTA) in solutions. The problem is partially solved for aqueous solutions; however, addition of another solvent, as an extra parameter to change the conditions of IPTA existence, significantly increases the opportunities to obtain information about particles, including those which do not exist in aqueous solutions or which cannot be isolated from them.

Decatungstate $W_{10}O_{32}^{4-}$ is most stable in mixed aqueous-organic solutions compared to all other IPTAs. It is supposed [2] that $W_{10}O_{32}^{4-}$ exists in equilibrium with Lindqvist hexatungstate anion $W_6O_{19}^{2-}$ in solution. The presence of dimethylformamide (DMF) in the system [3] almost completely shifts the equilibrium $5W_{12}O_{38}(OH)_2^{6-} + 6H^+ \rightleftarrows 6W_{10}O_{32}^{4-} + 8H_2O$ towards decatungstate anion, which is not the case in aqueous solutions [4].

Such behavior of IPTA in mixed solvents attracts interest also due to the unique photocatalytic properties of decatungstate that make it a perspective instrument in organic synthesis. Catalytic systems and conditions of photocatalysis, and kinetic and mechanistic aspects of catalysis have been studied over the last decades [5].

It should be noted that most decatungstates, which were synthesized and examined for their catalytic or other properties, are salts with organic cations (mostly tri- and tetrabutylammonium, trimethylammonium, and N-butylpyridinium [6–10]). Methods for decatungstate synthesis with inorganic cations are limited [4], although their advantage may be greater thermal stability that can extend the temperature limit of catalysis by these salts.

Sparingly soluble isopoly tungstates $Ba_5[W_{12}O_{40}(OH)_2]\cdot 22H_2O$, $Ba_5[HW_7O_{24}]_2\cdot 28H_2O$, and $Ba_3[W_{12}O_{38}(OH)_2]\cdot 23H_2O$ were isolated from aqueous solutions under appropriate acidities [11]. This allowed us to suggest that barium (II) is a good precipitating agent for IPTA.

The present article is aimed at studying the behavior of IPTA in aqueous DMF solutions, synthesis of crystalline barium (II) decatungstate from aqueous DMF medium, and characterization of its structure and properties.

2. Experimental

2.1. *pH-potentiometric studies*

Investigation of interactions in aqueous DMF solutions of sodium tungstate were carried out by pH-potentiometric titration by using hydrochloric acid in the region of acidity $Z = \nu(H^+)/\nu(WO_4^{2-}) = 0.0–2.5$ when the initial concentration of sodium tungstate $C_W = 10$ mM L^{-1} and ionic strength $\mu = 300$ mM L^{-1}. Ionic strength was created by the addition of the needed amount of 4 M L^{-1} solution of sodium chloride. Due to limited solubility of sodium tungstate in aqueous DMF solution [3], the solvent composition was limited to DMF concentration 50% (v/v), so the titrations were carried out in the systems with different DMF concentrations of 0, 10, 20, 30, 40, and 50% (v/v) (systems **I–VI**, respectively).

pH values (accuracy $\sigma \leq \pm 0.04$) were obtained using the I-160 (ZIP, Belarus) ionomer at 298.15 ± 0.10 K with the titration step $\Delta Z = 0.05$. Indicator electrode used was hydrogen-ion selective glass electrode ESL 63–07Sr (ZIP, Belarus) with the isopotential point pH_i 7.0 ± 0.3 pH and $E_i = -25 \pm 10$ mV, auxiliary electrode EVL–1M3 used was a silver chloride electrode (Ag/AgCl, sol. KCl, saturated) with the potential of 202 ± 2 mV compared to

the standard hydrogen electrode. Small temperature fluctuations were compensated by a thermocompensating apparatus (TCA 7.1). Calibration and preciseness of the readings were controlled by the standard buffer solutions – potassium tetraoxalate (KHC_2O_4) ($H_2C_2O_4$)·$2H_2O$ (pH 1.68), potassium hydrophthalate $KC_8H_5O_4$ (pH 4.01), and sodium tetraborate $Na_2B_4O_7$·$10H_2O$ (pH 9.18). pH values in the systems with appropriate content of organic solvent were obtained on the basis of the measured values ($pH_{Aq\text{-}DMF}$), with an account of the correction term Δ [0.02, 0.12, 0.22, 0.32, and 0.42 correspondingly for systems **II** (10% DMF), **III** (20% DMF), **IV** (30% DMF), **V** (40% DMF), and **VI** (50% DMF)], according to the equation: $pH = pH_{Aq\text{-}DMF} - \Delta$ [12, 13].

2.2. *Synthetic and analytical procedures*

To prepare Ba (II) IPTs, aqueous solutions of Na_2WO_4·$2H_2O$, $Ba(NO_3)_2$, HCl, and pure DMF (all reagent grade) were used. The precise concentrations of solutions were determined by chemical analysis: W contents – gravimetrically (gravimetric form WO_3, $\delta \leq \pm 0.5\%$); Ba contents – gravimetrically (gravimetric form $BaSO_4$, $\delta \leq \pm 0.5\%$); and HCl concentration – by titration of standard $Na_2B_4O_7$·$10H_2O$ solution ($\delta \leq \pm 0.5\%$).

The procedure for IPTs preparation was as follows. The solutions of sodium tungstate ($C_W = 100$ mM·L^{-1} and $V = 100$ mL) with DMF concentration 40% (v/v) were acidified with HCl to reach the acidity $Z = 1.60$, under which decatungstate anion was formed. Then a stoichiometric quantity of $Ba(NO_3)_2$ solution ($C_{Ba} = 300$ mM·L^{-1} and $V = 6.67$ mL) was added dropwise with vigorous stirring according to the equation:

$$2\ Ba^{2+} + 10\ WO_4^{2-} + 16\ H^+ \leftrightarrows Ba_2\ W_{10}O_{32} + 8H_2O$$

Furthermore, pH control was observed during the acidification, before Ba (II) addition and after the solid-phase isolation. The resulting precipitates were separated, washed with cold water, air dried, and analyzed as described below.

A 120 mg sample of each barium salt was refluxed in the mixture of 5 mL HNO_3 (70 wt %) and 15 mL HCl (36 wt%), and then evaporated using a water bath. Then, the wet residue was diluted with 70 mL of water and concentrated till 50 mL by evaporation on the water bath. The solid phase, WO_3·xH_2O, was filtered, washed with 3% aqueous solution of HNO_3, air dried and, finally, annealed at 800 °C to obtain a constant mass (gravimetric form WO_3, $\delta \leq \pm 0.5\%$).

The sodium in the filtrate was determined by atomic absorption spectroscopy, using Saturn-3 spectrometer. Acetylene-air flame with an analytical line of 589.6 nm was used and an electrodeless high-frequency lamp VSB–2 ($I = 70$ mA) served as a source of resonance irradiation.

The contents of barium in the filtrate were determined gravimetrically. First, the filtrate was evaporated to ~100 mL using a water bath. After that it was cooled, and 5 mL of H_2SO_4 (98 wt%) was added. The solution containing white crystalline precipitate $BaSO_4$ was concentrated and filtered, washed with 3% aqueous solution of H_2SO_4, air dried, and finally annealed at 800 °C to obtain a constant mass (gravimetric form $BaSO_4$, $\delta \leq \pm 0.5\%$).

The contents of the water and DMF (totally) in Ba (II) IPTs were determined gravimetrically by annealing air-dried samples at 550 °C ($\delta \leq \pm 0.5\%$).

To identify the anions in the synthesized salts, we used FTIR spectra that were recorded for KBr pellets on a Spectrum BX II (PerkinElmer) spectrometer from 400 to 4000 cm^{-1}. The contents of the sample in KBr matrix was 0.5 wt%.

Absorption spectrum for $[Ba(H_2O)_2(C_3H_7NO)_3]_2[W_{10}O_{32}]\cdot(C_3H_7NO)_2$ aqueous solution was obtained using a double-beam spectrophotometer, SF (2000), and from $\lambda = 200$ to 1000 nm. The solutions were placed into a quartz cuvette with an absorbing layer thickness of 10 mm and the spectrum was recorded with respect to pure distilled water.

Single-crystal X-ray analysis of $[Ba(H_2O)_2(C_3H_7NO)_3]_2[W_{10}O_{32}]\cdot(C_3H_7NO)_2$ was carried out on a Xcalibur-3 (Oxford Diffraction) diffractometer (Mo-Kα radiation, $\lambda = 0.71073$ Å, and graphite monochromator) equipped with Sapphire–3 CCD detector (ω/θ–scanning in the range $6.32 \leq 2\theta \leq 73.22$ with $-19 (h (18$, $-20 \leq k \leq 19$, $-21 \leq l \leq 17$, 26, and 454 measured reflections). The structure was solved by direct methods using SHELX-97 program package [14]. The hydrogens were located geometrically and refined in the riding model (in DMF), or with the geometrical limitations on the bond lengths (in H_2O). Structural analysis and image making were performed in WinGX [15] and Ball&Stick [16] applications, respectively.

X-ray diffraction patterns were obtained using a diffractometer, Siemens D500, Cu-Kα radiation, Ni filter, scanning with step 0.02° in the angle range $5° \leq 2\theta \leq 80°$, accumulation time 12 s in every point. Refinement of diffraction pattern was carried out by the Rietveld method (FullProf program [17]).

Scanning electronic (raster) microscopy and EDX analysis (JSM-6490 LV SEM with the use of aluminum stand and carbon film as the support) were used to investigate the surface morphology and prove the single-phase of triturated sample of $[Ba(H_2O)_2(C_3H_7NO)_3]_2[W_{10}O_{32}]\cdot(C_3H_7NO)_2$.

The thermal decomposition of $[Ba(H_2O)_2(C_3H_7NO)_3]_2[W_{10}O_{32}]\cdot(C_3H_7NO)_2$ was carried out in a Q-1500 derivatograph with a programed rate of heating at 5 °C/min from 20 to 800 °C.

3. Results and discussion

3.1. *Analysis of IPTs in the systems WO_4^{2-}–H^+–DMF–H_2O*

To obtain information about the particles present in the aqueous DMF solutions of sodium tungstate at different acidities, single-point pH-potentiometric titration was carried out. Titration data allowed to build $pH = f(Z)$ dependencies for systems **I**–**VI** (figure 1) with different DMF concentrations. The titration curves for systems **II**–**VI** have two inflections, at $Z = 1.00$–1.20 and 1.40–1.70, which are supposedly caused by hepta- and decatungstate anion formation. As a consequence of the significant basicity of polar aprotic solvents, the titration curves shift towards alkaline region as the DMF concentration increases.

Based on the titration results, mathematical modeling of the processes in the systems WO_4^{2-}–H^+–DMF–H_2O was carried out by the quasi–Newton method using CLINP 2.1 software [18, 19]. The target goal of mathematical modeling for the chemical processes in the system WO_4^{2-}–H^+–DMF–H_2O was to successively find such a model that adequately describes physicochemical measurements in the form of a material balance equation. First, the set of the most probable chemical reactions was created, and then by sequential exclusion, only those reactions that enhanced (or diminished) the calculated criterial parameters were left in the model. The main parameter was the value of F that is the sum of squares of deviations between calculated (calc) and experimental (exp) values of pH along the entire titration curve:

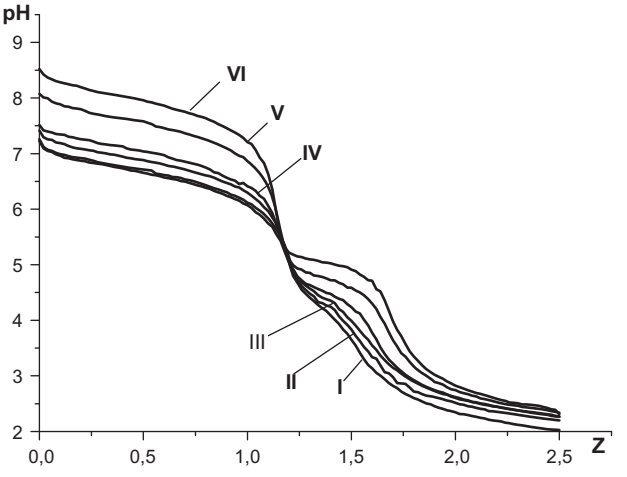

Figure 1. Experimental (points) and calculated (lines) (by CLINP 2.1) pH = $f(Z)$ dependencies for the systems WO_4^{2-}–H^+–DMF–H_2O (DMF concentration, % (v/v): 0 **(I)**, 10 **(II)**, 20 **(III)**, 30 **(IV)**, 40 **(V)**, 50 **(VI)**).

$$F = \sum_{k=1}^{n} (\Delta \mathrm{pH}_k)^2 = \sum_{k=1}^{n} \left(\mathrm{pH}_k^{(\mathrm{calc})} - \mathrm{pH}_k^{(\mathrm{exp})}\right)^2$$

where n is the number of points in the series of interest, $k = 1, 2, \ldots n$.

The calculated model was considered to be successful, if the calculated values of pH deviated from experimental values by ±0.12 in each titration point. The result of mathematical modeling was the determination of concentration formation constants ($\lg K_c$) of individual IPTAs in the solution (table 1).

Calculation of formation constants allowed us to build the diagrams (α, M.% = $f(Z)$) for the distribution of different ionic forms depending on acidity Z in the systems with different DMF concentrations [figure 2(a)–(f)]. The obtained diagrams of IPTA distribution show that $HW_7O_{24}^{5-}$ particles transform into $W_{12}O_{40}(OH)_2^{10-}$ after 10% (v/v) of DMF addition to the aqueous system. Increasing DMF concentration leads to the transformation of paratungstate B into heptatungstate anion ($W_7O_{24}^{6-}$ and $HW_7O_{24}^{5-}$). Protonated forms of paratungstate B ($H_xW_{12}O_{40}(OH)_2^{(10-x)-}$) exist in systems with all DMF concentrations, but x declines as medium polarity decreases. ψ-metatungstate ($W_{12}O_{38}(OH)_2^{6-}$) is hardly formed in the solutions with DMF content increasing and entirely disappears from systems **V** and **VI**. In all DMF containing systems (**II**–**VI**) under acidity of 1.60 decatungstate anion is formed, and in systems **V** and **VI** its protonated forms - $H_nW_{10}O_{32}^{(4-n)-}$ ($n = 1, 2$) – appear. The maximum mole fraction of $W_{10}O_{32}^{4-}$ at $Z = 1.60$ is formed in system **V**. Together with decatungstate anion, hydroheptatungstate and protonated forms of decatungstate anion are present at this acidity. Absence of ψ-metatungstate (its formation acidity being close to the formation acidity of decatungstate) in system **V** makes it impossible for salt admixtures to be formed during the decatungstate synthesis.

To reveal the optimal conditions for decatungstate synthesis, it was necessary to investigate the transformations, which occur with anions in system **V** at different time intervals after beginning the interaction. Based on the analysis of pH changes in the system and modeling using CLINP 2.1 program, the diagrams of IPTA distribution were built that allowed

Table 1. Concentrational constants of the formation of IPTA.

Anions	Z	lgK_c (S)* of anion formation					
		I	II	III	IV	V	VI
$W_6O_{20}(OH)_2^{6-}$	1.00	50.23 (0.30)	51.65 (0.37)	52.38 (0.37)	54.05 (0.39)	56.09 (0.85)	58.30 (0.64)
$W_7O_{24}^{6-}$	1.14	–	–	–	–	72.85 (0.97)	76.63 (0.77)
$W_{12}O_{40}(OH)_2^{10-}$	1.17	117.52 (0.86)	120.28 (0.88)	122.12 (0.88)	125.71 (0.89)	129.93 (0.97)	134.73 (0.88)
$HW_{12}O_{40}(OH)_2^{9-}$	1.25	120.93 (0.45)			130.63 (0.98)	134.88 (0.88)	–
$HW_7O_{24}^{5-}$	1.29	71.63 (0.90)	73.03 (0.87)	74.14 (0.91)	75.91 (0.99)	78.96 (0.93)	81.94 (0.90)
$H_2W_{12}O_{40}(OH)_2^{8-}$	1.33	–	–	131.11 (0.87)	–	–	–
$H_3W_{12}O_{40}(OH)_2^{7-}$	1.42	–	134.08 (0.80)	–	–	–	–
$W_{12}O_{38}(OH)_2^{6-}$	1.50	135.91 (0.88)	138.49 (0.84)	140.58 (0.84)	144.61 (0.94)	–	–
$HW_{12}O_{38}(OH)_2^{5-}$	1.58	139.02 (0.81)	–	–	–	–	–
$W_{10}O_{32}^{4-}$	1.60	– –	118.54 (0.87)	120.58 (0.85)	124.13 (0.83)	128.37 (0.86)	133.88 (0.90)
$HW_{10}O_{32}^{3-}$	1.70	– –	– –	123.53 (0.80)	127.73 (0.88)	131.56 (0.79)	138.24 (0.75)
$H_2W_{10}O_{32}^{3-}$	1.80	–	–	–	–	135.91 (0.82)	142.32 (0.91)
F		0.045	0.086	0.073	0.061	0.134	0.140
F/n		0.001	0.001	0.001	0.001	0.002	0.002

*S denotes a mean square deviation.

us to follow the changes in decatungstate concentration in system **V** over three weeks from the beginning of interaction.

As presented in figure 3, the decatungstate concentration decreases in the course of time; therefore, it is reasonable to synthesize decatungstates from a freshly prepared solution with acidity $Z = 1.60$ and DMF concentration 40% (v/v). At the same time, $W_{10}O_{32}^{4-}$ content does not fall lower than 45 molar % even after prolonged maturation period and decatungstate anion remains dominant in the solution. The last observation makes it possible to synthesize decatungstates also from solutions, which were matured for long time periods, very important for obtaining single-crystal samples.

3.2. *System with DMF concentration 40 % (v/v) and with acidity Z = 1.60*

pH-potentiometric data were used as a basis to obtain Ba (II) decatungstate. For this purpose, the acidity $Z = 1.60$ (pH 3.63, 298 K) was created in the solution with DMF concentration 40% (v/v) and by the addition of hydrochloric acid to the solution of sodium tungstate ($C_W = 100$ mM L^{-1}); after the addition of barium nitrate, formation of a small amount of white precipitates was observed and pH lowered from 3.31 to 2.98. After holding of the mother liquid at an ambient temperature (*ca.* 293 K) for a week, the precipitate $Ba_2H_2W_7O_{24}{\cdot}15H_2O$ (**1**) was filtered, washed with cold water, and air dried. Anal. Calcd for **1**: BaO, 13.83; WO_3, 73.18; and H_2O, 13.00. Found: BaO, 13.78; WO_3, 73.09; and H_2O, 12.92. FTIR spectrum of the sample does not contain DMF bands; however, bands at

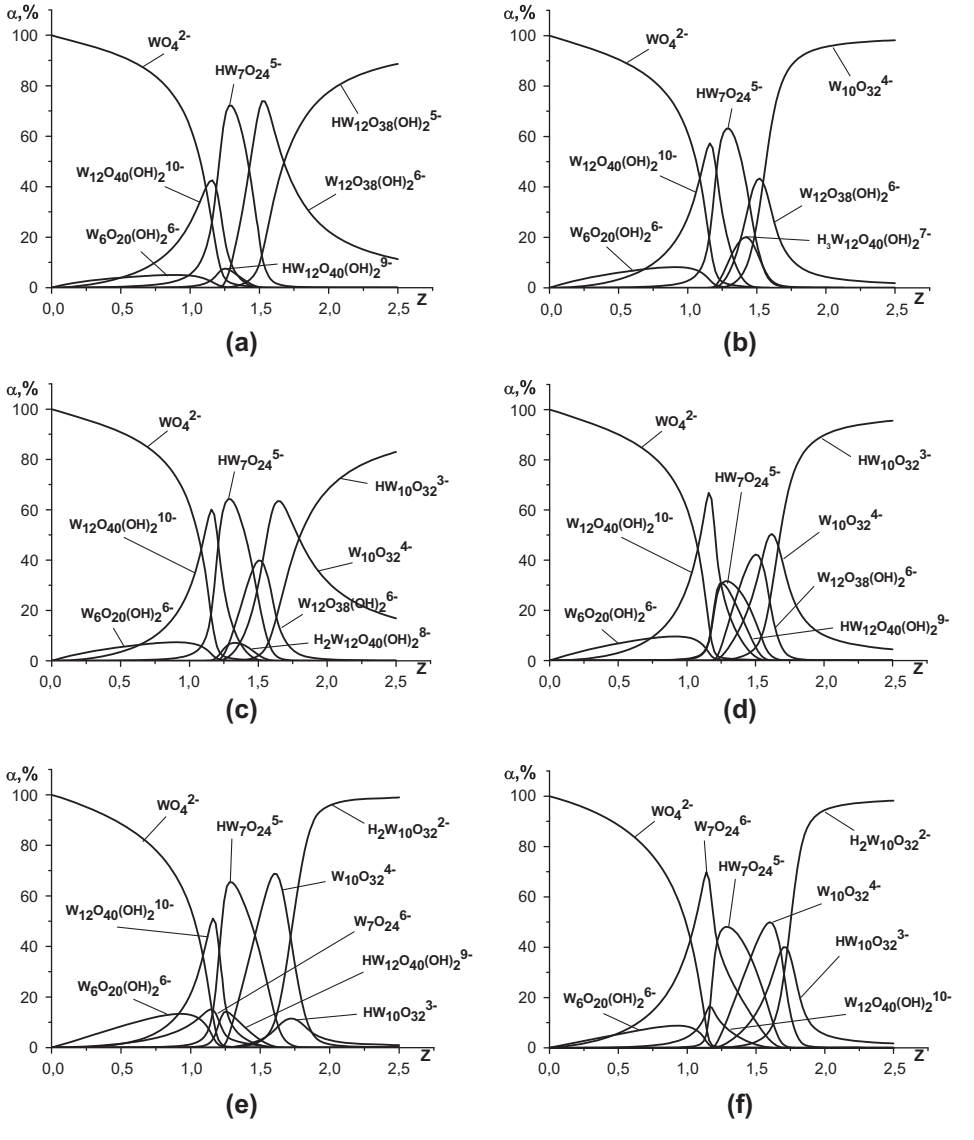

Figure 2. Calculated diagrams of IPTA α, M.% = $f(Z)$ distribution for the systems WO_4^{2-}–H^+–DMF–H_2O I (a), II (b), III (c), IV (d), V (e), and VI (f).

1630 and 3435 cm^{-1} indicate the presence of the water molecules. The tungsten oxide framework vibrations (ν(W-O-W) 509 w, 712 s, 829 s, 880 s, and ν(W=O) 943 s cm^{-1}) indicate that the anion present in the salt is heptatungstate and the bands are characteristic both in location and intensity [20].

After separation of **1,** the mother liquor was concentrated by evaporation on the water bath (373 K) from 100 to *ca.* 50 mL and was kept for a month at an ambient temperature (*ca.* 293 K) that caused precipitation of another white powder sediment $Ba_2H_2W_7O_{24}{\cdot}13H_2O$ (**2**). Anal. Calcd for **2**: BaO, 14.06; WO_3, 74.38; and H_2O, 11.56. Found:

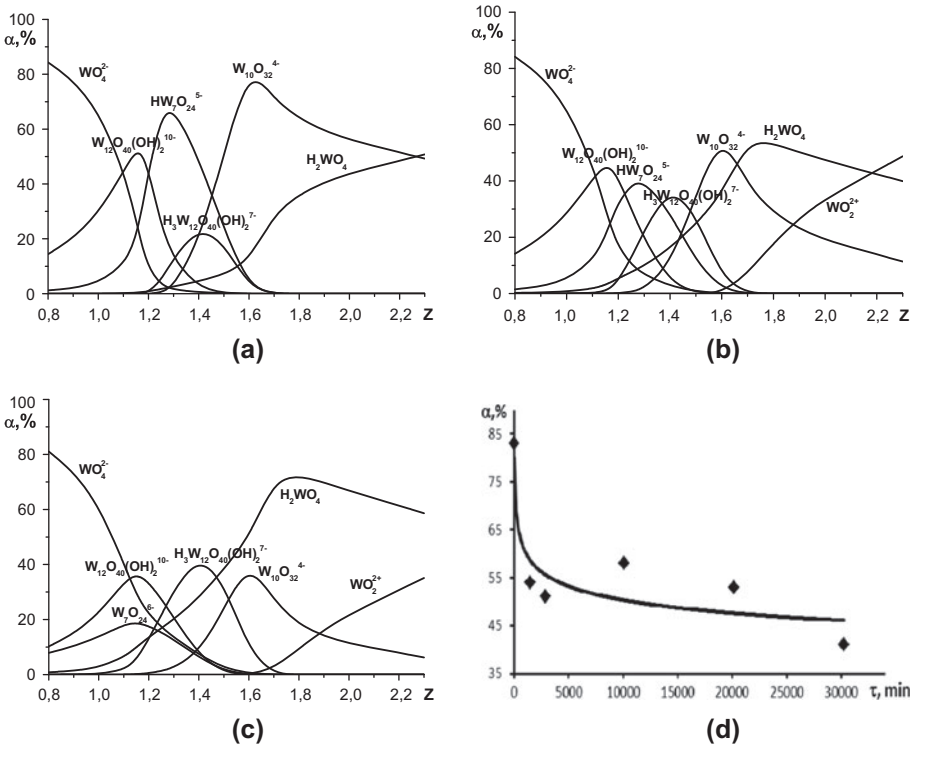

Figure 3. Calculated diagrams of IPTA α, M.% = $f(Z)$ distribution for the system **V** in different time intervals after the beginning of interaction: 30 min (a), 10,080 min (b), 30,240 min (c). Changes in $W_{10}O_{32}^{4-}$ molar content in different time intervals after the beginning of interaction (d).

BaO, 13.98; WO_3, 74.29; and H_2O, 11.50. FTIR spectrum (in KBr), cm^{-1}: δ(W-O-W) 414 w, 436 w, ν(W-O-W) 508 w, 714 s, 821 s, 876 s, ν(W=O) 933 s, (W-OH) 1081 w, $\delta(H_2O)$ 1628 s, and $\nu(H_2O)$ 3435 br s. Both powder phases, separated from the system at $Z = 1.60$, are heptatungstates and do not contain DMF, but contain H_2O molecules.

On the following day after separation of **2,** yellowish-white transparent crystals $[Ba(H_2O)_2(C_3H_7NO)_3]_2[W_{10}O_{32}]\cdot(C_3H_7NO)_2$ (**3**) formed in the mother liquor (293 K). When triturated, the crystals of **3** become blue if placed in straight sunlight that is typical for salts with decatungstate anion [21]. Anal. Calcd for **3**: BaO, 9.34; WO_3, 70.64; ($H_2O + C_3H_7ON$), and 20.02. Found: BaO, 9.44; WO_3, 70.26; ($H_2O + C_3H_7ON$), and 19.89. FTIR spectrum (in KBr), cm^{-1}: δ(W-O-W) 410 w, 436 m, ν(W-O–W) 580 m, 801 s, 890 s, ν(W=O) 968 s, δ(W-O–H) 1061 w, 1108 m, δ(C–N–C) 1251 m, δ(H-C–H) 1438 m, ν(C–N) 1500 m, $\delta(H_2O)$ 1640 s, ν(C=O) 1667, ν(C–H) 2812 w, 2875 w, 2933 w, 2972 w, and $\nu(H_2O)$ 3497 br s. Crystalline phase **3**, as opposed to previous phases **1** and **2**, contains DMF molecules (bands at 1116–2972 cm^{-1}) (figure 4).

Solutions containing decatungstate anion have maximum absorption spectrum at 320–325 nm [22]. It is interesting to note that the only IPTA which has a signal in the range close to UV is decatungstate anion, which is related to its structure; anion $W_{10}O_{32}^{4-}$ is made up of two lacunar blocks W_5O_{18}, connected by almost linear bridges W–O–W (175°). The only other polytungstates with a charge transfer band as low as 325 nm are α- and

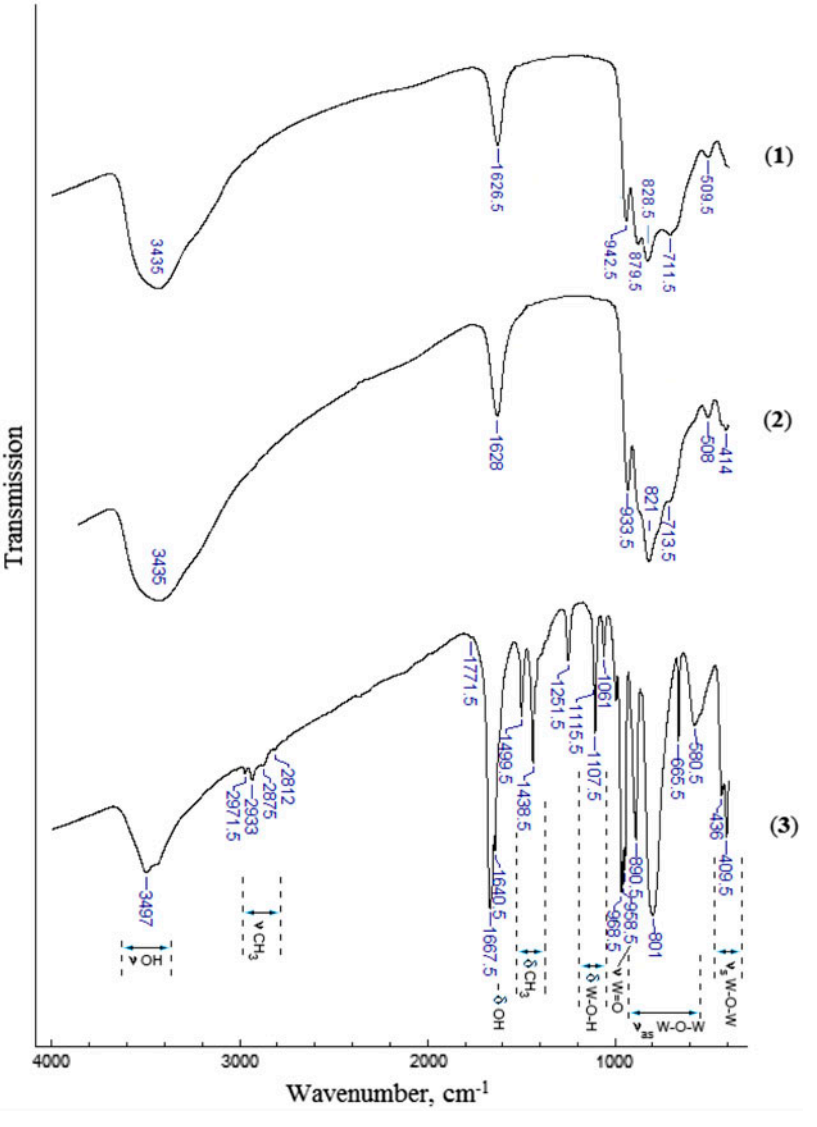

Figure 4. FT-IR-spectra of phases **1**, **2** and **3**, separated from the system at $Z = 1.60$.

β-$P_2W_{18}O_{62}^{6-}$, which also have dimeric structures, linked by almost linear (162°) W–O-W bridges [23]. Aqueous solution of **3** ($C_{(3)} = 0.5$ mM L^{-1}) has an absorption maximum at 319 nm that points to the presence of decatungstate anion in the salt.

SEM images of triturated **3** (figure 5) show that there are no zones with a different surface morphology. Twenty thousand times magnification shows that the surface is built of spherical granules 220–370 nm in size. EDX spectral analysis in different zones (figure 6), averaged for every sample (table 2), exhibited no substantial deviation from the molar ratio Ba : W = 1 : 5. This clearly indicates the formation of a monophase sample of $Ba_2W_{10}O_{32}\cdot 8C_3H_7NO\cdot 4H_2O$.

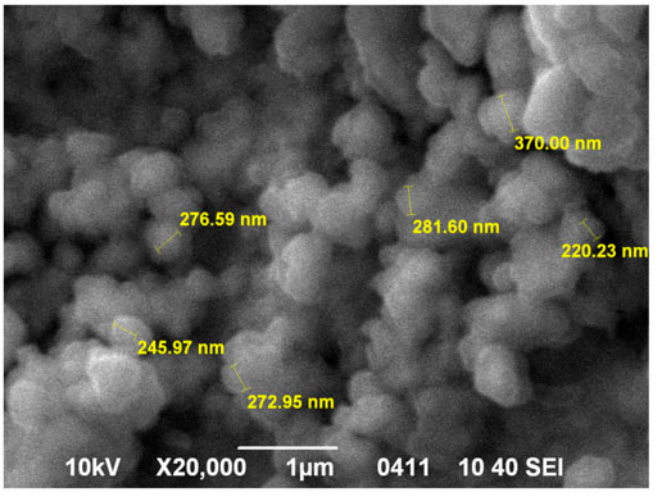

Figure 5. SEM image of the surface of triturated sample of **3** (×20,000 times).

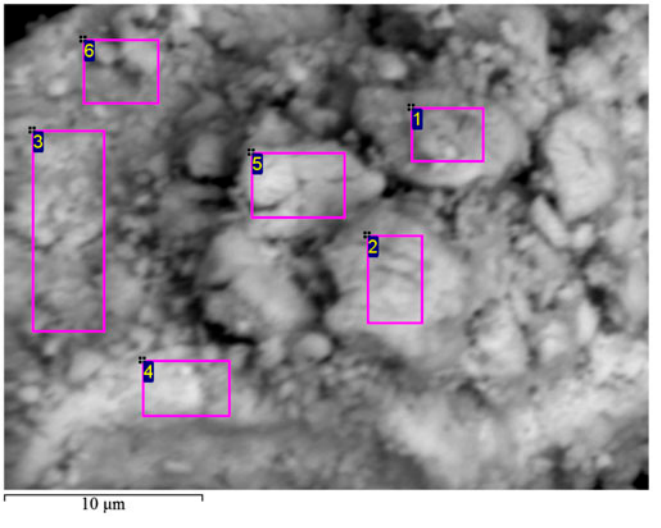

Figure 6. SEM images of the morphology of triturated **3**. EDX analysis was made in the zones indicated (table 2).

Table 2. Atomic ratio of Ba and *W* in different surface zones of triturated **3**.

	Zones							$\nu_{Ba} : \nu_W$	
W, at.%	1	2	3	4	5	6	Average	Exp.	Theor.
Ba	5.14	5.17	5.06	5.16	5.03	4.63	5.03	1	1
W	24.89	25.53	24.44	25.26	25.03	23.28	24.74	4.92	5

Table 3. Crystallographic data and structure refinement parameters of **3**.

Empirical formula	$C_{24}H_{64}Ba_2N_8O_{44}W_{10}$
Formula weight	3282.01
Crystal system	Triclinic
Space group	*P–1*
T (K)	293(2)
Wavelength (Å)	0.71073
a (Å)	11.899(3)
b (Å)	12.1313(11)
c (Å)	13.341(2)
α (°)	70.417(11)
β (°)	64.254(18)
γ (°)	87.185(12)
Volume (Å^3), *Z*	1623.75(5), 1
Calculated density (g cm^{-3})	3.356
Absorption coefficient (mm^{-1})	18.920
F (0 0 0)	1468
Total reflections	26,454
Independent reflections	14,686 [*R*(int) = 0.047]
Final *R* indices [I_{hkl}> $2\sigma(I)$]	R_F = 0.0435, wR_2 = 0.0687 (for the observed reflections) R_F = 0.0764, wR_2 = 0.0787 (for all independent reflections)
S	0.981

Table 4. Bond distances (Å) in **3**.

Bond distances (Å)*					
W(1)–O(1)	1.715(3)	W(3)–O(11)	1.916(2)	W(5)–O(14)	1.914(2)
W(1)–O(3)	1.895(3)	W(3)–O(6)	1.916(2)	W(5)–O(2)	1.952(3)
W(1)–O(4)	1.914(3)	W(3)–O(4)	1.947(3)	W(5)–O(9)	2.318(3)
W(1)–O(2)	1.914(3)	W(3)–O(9)	2.337(3)	Ba(1)–O(17)	2.649(4)
W(1)–O(5)	1.926(2)	W(4)–O(15)	1.709(2)	Ba(1)–O(1)	2.768(3)
W(1)–O(9)	2.272(3)	W(4)–O(10)#1	1.881(3)	Ba(1)–O(19)	2.775(5)
W(2)–O(7)	1.706(3)	W(4)–O(14)	1.911(3)	Ba(1)–O(20)	2.775(4)
W(2)–O(6)	1.905(3)	W(4)–O(11)	1.914(3)	Ba(1)–O(18)#2	2.798(4)
W(2)–O(10)	1.908(3)	W(4)–O(3)	1.955(3)	Ba(1)–O(7)#3	2.807(3)
W(2)–O(8)	1.915(3)	W(4)–O(9)	2.288(2)	Ba(1)–O(21)	2.884(3)
W(2)–O(5)	1.917(3)	W(5)–O(16)	1.696(4)	Ba(1)–O(18)	2.888(3)
W(2)–O(9)	2.316(2)	W(5)–O(13)#1	1.900(3)	Ba(1)–O(21)#2	3.026(4)
W(3)–O(12)	1.698(4)	W(5)–O(8)	1.914(2)	Ba(1)–Ba(1)#2	4.0608(10)
W(3)–O(13)	1.890(3)				

*Symmetry operations needed to obtain equivalent atoms: #1 $-x+2, -y+1, -z+1$; #2 $-x+1, -y+2, -z+2$; #3 $-x+2, -y+2, -z+1$.

Single-crystal X-ray diffraction analysis was carried out for **3** to confirm the presence of decatungstate anion in the structure. Crystals, suitable for analysis, were isolated from the solution, air dried, and then used for crystal structure description. The structure was solved by direct methods using SHELX-97 software package [14]. Selected crystal parameters of **3** are summarized in table 3. Main geometrical characteristics and hydrogen bonds for the structure of **3** are depicted in tables 4–6.

Two lacunar derivatives from the Lindquist structure units W_5O_{18} in the centrosymmetrical decatungstate anion $W_{10}O_{32}^{4-}$ are bonded mirror-symmetrically through common tops of four oxygens with the formation of an octahedral space (figure 7). The polyanion contains four different groups of oxygens: 10 terminal (O_t = O(1), O(7), O(12), O(15), O(16),

Table 5. Bond angles (°) for **3**.

Bond angles (°)*			
O(1)–W(1)–O(3)	103.74(12)	O(10)#1–W(4)–O(9)	88.35(10)
O(1)–W(1)–O(4)	103.75(16)	O(14)–W(4)–O(9)	76.24(10)
O(3)–W(1)–O(4)	87.85(13)	O(11)–W(4)–O(9)	76.93(10)
O(1)–W(1)–O(2)	101.97(15)	O(3)–W(4)–O(9)	75.20(10)
O(3)–W(1)–O(2)	87.23(13)	O(16)–W(5)–O(13)#1	100.50(16)
O(4)–W(1)–O(2)	154.24(12)	O(16)–W(5)–O(8)	104.30(13)
O(1)–W(1)–O(5)	102.84(12)	O(13)#1–W(5)–O(8)	89.11(11)
O(3)–W(1)–O(5)	153.39(12)	O(16)–W(5)–O(14)	103.52(13)
O(4)–W(1)–O(5)	87.11(12)	O(13)#1–W(5)–O(14)	88.62(11)
O(2)–W(1)–O(5)	86.07(12)	O(8)–W(5)–O(14)	152.04(13)
O(1)–W(1)–O(9)	178.81(14)	O(16)–W(5)–O(2)	95.41(15)
O(3)–W(1)–O(9)	76.69(10)	O(13)#1–W(5)–O(2)	164.08(14)
O(4)–W(1)–O(9)	77.35(12)	O(8)–W(5)–O(2)	87.77(11)
O(2)–W(1)–O(9)	76.91(11)	O(14)–W(5)–O(2)	86.85(11)
O(5)–W(1)–O(9)	76.71(10)	O(16)–W(5)–O(9)	170.48(13)
O(7)–W(2)–O(6)	102.78(15)	O(13)#1–W(5)–O(9)	88.97(12)
O(7)–W(2)–O(10)	98.10(13)	O(8)–W(5)–O(9)	76.65(11)
O(6)–W(2)–O(10)	87.56(13)	O(14)–W(5)–O(9)	75.44(11)
O(7)–W(2)–O(8)	104.34(15)	O(2)–W(5)–O(9)	75.12(12)
O(6)–W(2)–O(8)	152.86(10)	O(17)–Ba(1)–O(1)	72.30(10)
O(10)–W(2)–O(8)	87.49(13)	O(17)–Ba(1)–O(19)	83.23(15)
O(7)–W(2)–O(5)	99.86(13)	O(1)–Ba(1)–O(19)	72.21(12)
O(6)–W(2)–O(5)	88.42(13)	O(17)–Ba(1)–O(20)	85.07(13)
O(10)–W(2)–O(5)	162.04(10)	O(1)–Ba(1)–O(20)	66.29(11)
O(8)–W(2)–O(5)	88.14(13)	O(19)–Ba(1)–O(20)	138.49(12)
O(7)–W(2)–O(9)	175.57(13)	O(17)–Ba(1)–O(18)#2	135.30(14)
O(6)–W(2)–O(9)	76.38(10)	O(1)–Ba(1)–O(18)#2	131.63(9)
O(10)–W(2)–O(9)	86.23(10)	O(19)–Ba(1)–O(18)#2	135.62(13)
O(8)–W(2)–O(9)	76.67(10)	O(20)–Ba(1)–O(18)#2	76.61(11)
O(5)–W(2)–O(9)	75.81(10)	O(17)–Ba(1)–O(7)#3	143.20(12)
O(12)–W(3)–O(13)	99.29(16)	O(1)–Ba(1)–O(7)#3	71.94(9)
O(12)–W(3)–O(11)	104.33(13)	O(19)–Ba(1)–O(7)#3	77.94(11)
O(13)–W(3)–O(11)	88.59(11)	O(20)–Ba(1)–O(7)#3	88.45(10)
O(12)–W(3)–O(6)	104.30(14)	O(18)#2–Ba(1)–O(7)#3	77.32(10)
O(13)–W(3)–O(6)	88.98(12)	O(17)–Ba(1)–O(21)	126.11(11)
O(11)–W(3)–O(6)	151.28(14)	O(1)–Ba(1)–O(21)	141.02(10)
O(12)–W(3)–O(4)	96.79(15)	O(19)–Ba(1)–O(21)	76.31(12)
O(13)–W(3)–O(4)	163.92(14)	O(20)–Ba(1)–O(21)	139.77(11)
O(11)–W(3)–O(4)	87.05(12)	O(18)#2–Ba(1)–O(21)	63.35(11)
O(6)–W(3)–O(4)	87.45(11)	O(7)#3–Ba(1)–O(21)	79.56(9)
O(12)–W(3)–O(9)	171.96(14)	O(17)–Ba(1)–O(18)	69.76(11)
O(13)–W(3)–O(9)	88.75(12)	O(1)–Ba(1)–O(18)	138.06(10)
O(11)–W(3)–O(9)	75.68(11)	O(19)–Ba(1)–O(18)	86.10(11)
O(6)–W(3)–O(9)	75.66(11)	O(20)–Ba(1)–O(18)	126.20(11)
O(4)–W(3)–O(9)	75.17(12)	O(18)#2–Ba(1)–O(18)	88.86(9)
O(15)–W(4)–O(10)#1	99.35(13)	O(7)#3–Ba(1)–O(18)	138.75(10)
O(15)–W(4)–O(14)	103.57(14)	O(21)–Ba(1)–O(18)	59.67(9)
O(10)#1–W(4)–O(14)	89.77(13)	O(17)–Ba(1)–O(21)#2	76.43(13)
O(15)–W(4)–O(11)	103.02(14)	O(1)–Ba(1)–O(21)#2	125.67(10)
O(10)#1–W(4)–O(11)	89.50(13)	O(19)–Ba(1)–O(21)#2	145.22(9)
O(14)–W(4)–O(11)	153.17(10)	O(20)–Ba(1)–O(21)#2	67.78(9)
O(15)–W(4)–O(3)	97.10(13)	O(18)#2–Ba(1)–O(21)#2	58.93(9)
O(10)#1–W(4)–O(3)	163.55(10)	O(7)#3–Ba(1)–O(21)#2	133.42(9)
O(14)–W(4)–O(3)	86.23(13)	O(21)–Ba(1)–O(21)#2	93.24(10)
O(11)–W(4)–O(3)	86.95(13)	O(18)–Ba(1)–O(21)#2	60.57(11)
O(15)–W(4)–O(9)	172.30(13)		

*Symmetry operations needed to obtain equivalent atoms: #1 $-x+2, -y+1, -z+1$; #2 $-x+1, -y+2, -z+2$; #3 $-x+2, -y+2, -z+1$.

Table 6. Characteristics of hydrogen bonds D–H···A in the structure of **3**.

	Distance, Å				
D–H···A	d(D–H)	d(H···A)	d(D···A)	Angle DHA, °	Coordinates of atom A
O(20)–H(20A)···O(2)	0.851(7)	2.086(7)	2.911(5)	163.0(13)	x, y, z
O(20)–H(20B)···O(22)	0.850(7)	1.935(7)	2.767(6)	166.1(16)	x, y, z
O(21)–H(21A)···O(15)	0.849(6)	2.112(8)	2.930(4)	161.7(15)	$x, y+1, z$
O(21)–H(21B)···O(22)	0.850(7)	2.062(9)	2.887(6)	163.4(11)	$-x+1, -y+2, -z+2$

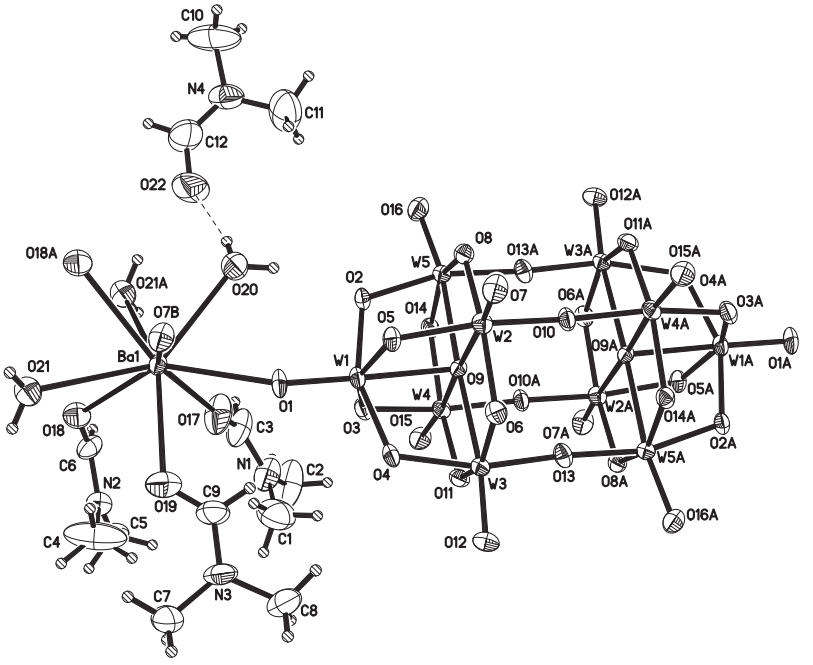

Figure 7. Main structural unit of **3**. Symmetry equivalent atoms are marked as "A" and "B".

and their symmetry equivalent atoms), 16 bridging (O_b = O(2)–O(6), O(8), O(11), O(14), and their symmetry equivalent atoms), each bridging two W ions through the edges of octahedra, four (O_e = O(10), O(13), O(10A), and O(13A)) bridging two tungstens through the corners of octahedra, and two [O_c = O(9) and O(9A)] each coordinated to five tungstens. The W – O distances within the polyanion are: W – O_t = 1.696–1.715 Å, W – O_b = 1.895–1.955 Å, W – O_e = 1.881–1.908 Å, and W – O_c = 2.272–2.337 Å.

Octahedra WO_6 in $W_{10}O_{32}^{4-}$ are significantly distorted as indicated by both bond angles (theoretically right bond angles O – W – O vary within 75.12°–104.34°, and the angles in theoretically linear fragments vary from 151.28° to 178.81°).

Barium coordinated polyhedron is monocapped square antiprism, the bottom of which is formed by oxygens of H_2O O(21), carbonyl O(18) of one DMF and equivalent atoms O (21A) and O(18A); equatorial oxygens are O(17) and O(19) of two other DMF molecules, O(20) of a second H_2O and O(7B) from the anion; the terminal O(1) of the anion is in the top of the antiprism. The center of the antiprism bottom coincides with the symmetry

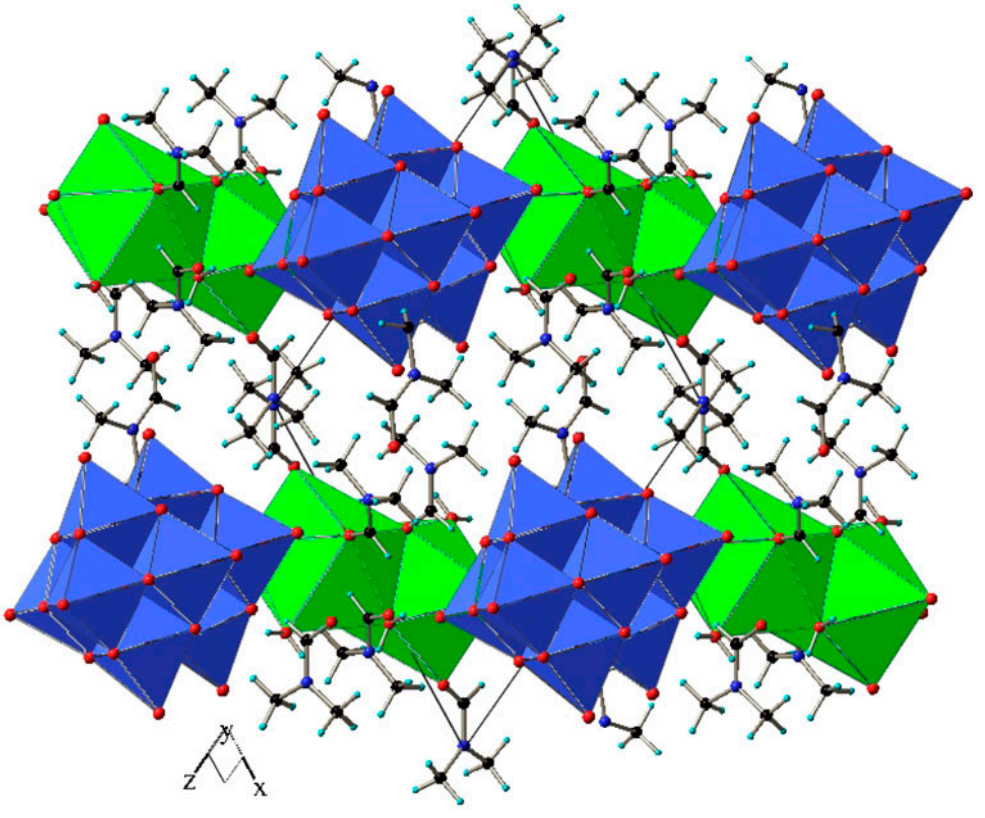

Figure 8. Projection of the structure of **3** along the [0 1 0] direction. Color codes: {BaO_9}, green polyhedron; {WO_6}, blue octahedron; C (black), N (blue), H (cyan) and O (red) atoms are shown with thick sticks (see http://dx.doi.org/10.1080/00958972.2014.987136 for color version).

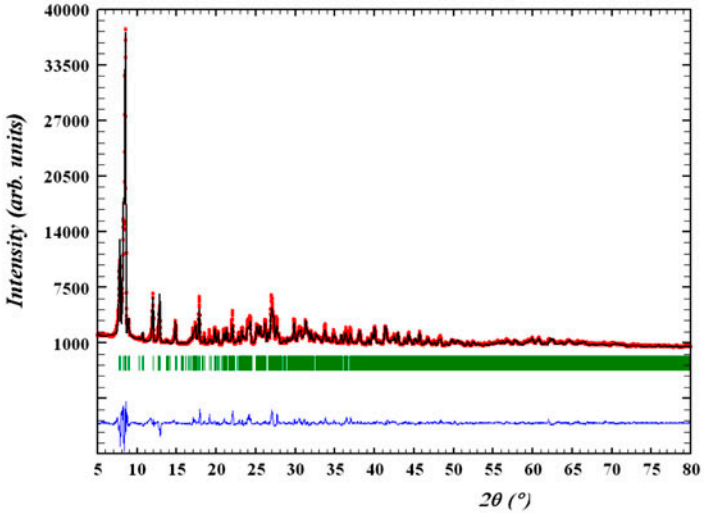

Figure 9. Powder X-ray diffraction pattern of **3**. Experimental values are shown by red circles; the solid curve was plotted as a result of the full profile refinement performed using the single crystal data (see http://dx.doi.org/10.1080/00958972.2014.987136 for color version).

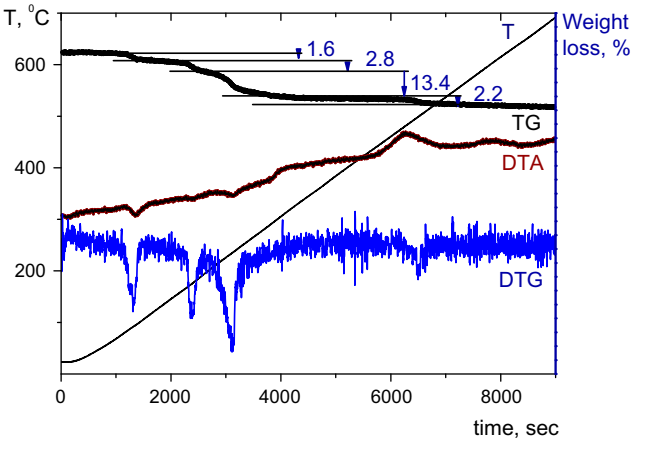

Figure 10. Thermal decomposition of **3** (curves: T stemperature, TG – thermogravimetric, DTG – differential thermogravimetric, DTA – differential thermal analysis).

center; therefore, two such monocapped antiprisms have a common bottom, forming a cationic cluster $[Ba(H_2O)_2(DMF)_3O_2]_2$. Another DMF is the crystallization and forms hydrogen bonds with two H_2O molecules in the structure. Cationic and anionic polyhedra in the structure of **3** are packed into layers that occupy crystallographic planes (1 0 1). Figure 8 shows projection of the structure along the [0 1 0] direction. On the basis of these data, the molecular formula of **3** is $[Ba(H_2O)_2(C_3H_7NO)_3]_2[W_{10}O_{32}]\cdot(C_3H_7NO)_2$.

As opposed to many polyoxotungstates, containing many water molecules in the independent part of the cell and losing the solvent during storage, **3** is rather stable even after trituration, which made it possible to obtain a powder X-ray diffraction pattern. The absence of admixture lines on the diffraction pattern (figure 9) exhibits that **3** is the only crystalline product of synthesis.

The thermal decomposition of **3** leads to several regions of mass loss (figure 10) due to the dehydration and desolvation of the compound: 75–100 °C (three H_2O molecules), 162–187 °C (one H_2O and one DMF), 212–244 °C (six DMF molecules), and 470–510 °C

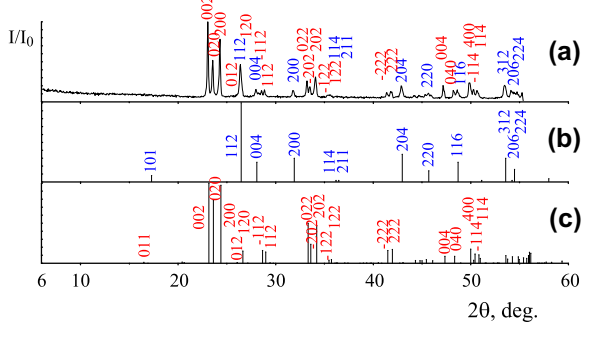

Figure 11. Powder X-ray diffraction patterns: (a) products of thermolysis of **3** (2 h at 550 °C); (b) $BaWO_4$ (ICDD PDF 00-008-0457); and (c) WO_3 (ICDD PDF 01-072-1465).

(one DMF molecule). On the DTA curve, the endothermic effects at T_{max} = 89, 175, and 233 °C are observed. An exothermic effect at T = 460–495 °C corresponds to the crystallization of WO_3 (ICDD PDF 01-072-1465 [24]) and $BaWO_4$ (ICDD PDF 00-008-0457 [24]), whose reflections are fixed on the X-ray diffraction pattern of thermolysis products (after annealing for 2 h at 550 °C) (figure 11).

4. Conclusion

The study of isopolytungstate anion formation and transformation in the systems with different DMF contents, WO_4^{2-}–H^+–DMF–H_2O allowed the determination of optimal conditions for decatungstate synthesis from aqueous DMF solutions: acidified to Z = 1.60 sodium tungstate solution with the concentration of DMF 40% (v/v). The synthesis under these conditions leads to the formation of crystalline barium decatungstate $[Ba(H_2O)_2(C_3H_7NO)_3]_2[W_{10}O_{32}]\cdot(C_3H_7NO)_2$.

Supplementary material

Tables of atomic coordinates, bond lengths and angles, anisotropic displacement parameters, hydrogen coordinates, and isotropic displacement parameters were deposited at the Cambridge Crystallographic Data Center under depository number CCDC 1018995 and can be obtained free of charge by contacting CCDC, 12 Union Road, Cambridge CB2 IEZ, UK (Fax:+44-1223-336-033; E-mail: deposit@ccdc.cam.ac.uk, or http://www.ccdc.cam.ac.uk).

Funding

The present study was financially supported by the Ministry of Education and Science of Ukraine [grant number 0113U001530].

References

[1] D.E. Katsoulis. *Chem. Rev.*, **98**, 359 (1998).
[2] M.T. Pope. *Heteropoly and Isopoly Oxometallates*., Springer-Verlag, Berlin (1983).
[3] G.M. Rozantsev, O.N. Lysenko, E.E. Belousova. *Zh. Neorg. Khim.*, **45**, 1761 (2000) (in Russian).
[4] S.V. Radio, M.A. Kryuchkov, E.G. Zavialova, V.N. Baumer, O.V. Shishkin, G.M. Rozantsev. *J. Coord. Chem.*, **63**, 1678 (2010).
[5] C. Tanielian. *Coord. Chem. Rev.*, 178–180, 1165 (1998).
[6] A. Chemseddine, C. Sanchez, J. Livage, J.P. Launay, M. Fournier. *Inorg. Chem.*, **23**, 2609 (1984).
[7] M.D. Tzirakis, I.N. Lykakis, M. Orfanopoulos. *Chem. Soc. Rev.*, **38**, 2609 (2009).
[8] S. Montanaro, D. Ravelli, D. Merli, M. Fagnoni, A. Albini. *Org. Lett.*, **14**, 4218 (2012).
[9] A. Molinari, R. Amadelli, V. Carassiti, A. Maldotti. *Eur. J. Inorg. Chem.*, **1**, 91 (2000).
[10] D. Liu, J. Gui, F. Lu, Z. Sun, Y.-K. Park. *Catal. Lett.*, **142**, 1330 (2012).
[11] S.V. Radio, V.O. Yeliakina, N.O. Melnik, G.M. Rozantsev. *Vopr. Khim. Khim. Techn.*, **5**, 127 (2012) (in Russian).
[12] V.V. Alexandrov. *Acidity of Nonaqueous Solutions*, Vyscha shkola, Kharkov (1981) (in Russian).
[13] G. Papanastasiou, I. Ziogas. *Anal. Chim. Acta*, **221**, 295 (1989).
[14] G.M. Sheldrick. *Acta Crystallogr., Sect. A*, **64**, 112 (2008).
[15] L.J. Farrugia. *J. Appl. Cryst.*, **32**, 837 (1999).
[16] T.C. Ozawa, S.J. Kang. *J. Appl. Cryst.*, **37**, 679 (2004).

[17] J. Rodriguez-Carvajal, T. Roisnel. *FullProf.98 and WinPLOTR: New Windows 95/NT Applications for Diffraction*. Commission for Powder Diffraction, International Union of Crystallography, Newsletter No. 20 (May–August) Summer (1998).
[18] Yu.V. Kholin. *Quantitative Physico–chemical Analysis of Complex Formation in Solutions and on the Surface of the Chemically Modified Silica: Models, Mathematical Methods and their Applications*., Folio, Kharkov (2000) (in Russian).
[19] S.A. Merny, D.S. Konyaev, Y.V. Kholin. *CLINP 2.1, A Program for Computation of Stability Constants and Physicochemical Parameters of Complex Compounds in Solutions, Extractional and Sorptional Systems on the Base of Composition–Property Dependencies*. Available online at: http://www-chemo.univer.kharkov.ua/kholin/clinp.html
[20] X.-F. Wang, J. Cao, K.-L. Huang, Y.-Q. Xu, Y.-N. Chi, C.-W. Hu. *Eur. J. Inorg. Chem.*, **2013**, 1788 (2013).
[21] Y. Song, Q. Huang, K. Yih-Tong, G. Yi-Dong. *Chin. J. Chem.*, **8**, 141 (1990).
[22] L. Lorente, M.A. Martinez, J.M. Arrieta, C. Santiago, A. Arnaiz. *Thermochim. Acta*, **98**, 89 (1986).
[23] S.C. Termes, M.T. Pope. *Inorg. Chem.*, **17**, 500 (1978).
[24] Powder Diffraction File. *Joint Committee on Powder Diffraction Standards*, International Centre for Diffraction Data, Newtown Square, PA (2005).